Mergos, P.E. & Kappos, A. J. (2015). Estimating fixed-end rotations of reinforced concrete members at yielding and ultimate. Structural Concrete, 16(4), pp. 537-545. doi: 10.1002/suco.201400067

CITY UNIVERSITY LONDON

City Research Online

Panagiotis E. Mergos
Andreas J. Kappos

Estimating fixed-end rotations of reinforced concrete members at yielding and ultimate

<Abstract: Strain-penetration of the longitudinal reinforcement of reinforced concrete (RC) members in the joints and/or footings results in fixed-end rotations at the member ends. Several experimental studies have shown that fixed-end rotations caused by strain-penetration contribute significantly (up to 50%) to the total displacement capacity of RC members. Hence, accurate determination of these fixed-end rotations at yielding and ultimate limit states becomes of primary importance when defining the structural response of RC members. The purpose of this study is to present the theoretical background and the assumptions behind the most common relationships found in the literature for determining strain-penetration induced fixed-end rotations at yielding and ultimate. Furthermore, new simple relationships are proposed on the basis of realistic and mechanically-based assumptions. Comparisons between the existing and proposed relationships demonstrate the limitations of the former. Finally, the proposed relationships are calibrated against experimental measurements of RC column specimens subjected to cyclic loading with recorded fixed-end rotations due to strain-penetration in the adjacent joints and/or footings.>

1   Introduction

Performance-based design increasingly gains ground in seismic design of RC structures. A basic prerequisite of reliable performance-based design of RC structures is the reliable knowledge of individual member lateral displacement at the threshold of different performance levels.

In general, for RC members, lateral displacement at yielding and ultimate can be considered as the sum of three individual components. The displacements originating from flexural and shear deformation mechanisms and the displacement due to strain-penetration of the longitudinal reinforcement at the beam-column joints and/or footings. Estimation of the latter displacement component represents the main focus of the study presented herein.

Several experimental studies have shown that fixed-end rotations caused by strain-penetration of longitudinal bars in the joints contribute significantly (up to 50%) to the total displacement capacity of RC members [1-3].

Various analytical methodologies have been developed so far for the determination of fixed-end rotations caused by strain-penetration in the anchorage zone. These methodologies range from the most elaborate and accurate, which use the finite element or finite difference method [4-6] to rather simplified ones, yet accurate enough, which assume prescribed distributions of bond stress along the anchorage length [7-13].

The main objective of this study is to propose new simple closed-form relationships for calculating anchorage slip rotations at yielding and ultimate. The proposed relationships are mechanics based, which assures that all main parameters affecting anchorage slip are taken sufficiently into consideration. The new relationships are calibrated against experimental measurements and are later used to evaluate widely adopted relationships from the literature.

2   Fixed-end rotation at yielding

If s denotes slippage of the tension reinforcement from its anchorage, fixed-end rotation θ_{slip} is given by Eq. (1), where x_c is the neutral axis depth and d is the effective depth of the member end section

$$\theta_{slip} = \frac{s}{d - x_c} \tag{1}$$

The most common assumption, when estimating fixed-end rotation at yielding, is that the bond stress τ_{be} is constant along an anchorage length L_{be} [7-13]. This assumption is convenient but does not accurately reflect the real phenomenon.

As shown in Fig. 1, when τ_{be} is assumed constant along L_{be}, bar stress $\sigma_s(x)$ increases linearly from zero at the end of L_{be} to the bar yield strength f_{yl} at the member end section. Since the bar remains in the elastic range, steel strains $\varepsilon_s(x)$ also increase linearly from zero to ε_y at the respective locations. Anchorage slip at yielding s_y can now easily be calculated by integration as

$$s_y = \int_0^{L_{be}} \varepsilon_s(x)\,dx = \frac{1}{2} \cdot \varepsilon_y \cdot L_{be} \tag{2}$$

The length L_{be} is determined by equilibrium for the bar with diameter d_{bl} as:

$$\pi \cdot d_{bl} \cdot L_{be} \cdot \tau_{be} = \pi \cdot \frac{d_{bl}^2}{4} \cdot f_{yl} \rightarrow L_{be} = \frac{d_{bl} \cdot f_{yl}}{4 \cdot \tau_{be}} \tag{3}$$

Combining Eqs. (1), (2) and (3), the fixed-end rotation at yielding $\theta_{y,slip}$ is obtained as a function of the curvature at yielding φ_y.

$$\theta_{y,slip} = \frac{s_y}{d - x_c} = \frac{1}{2} \cdot \frac{\varepsilon_y}{d - x_c} \cdot L_{be} = \varphi_y \cdot \frac{d_{bl} \cdot f_{yl}}{8 \cdot \tau_{be}} \tag{4}$$

One problem in the afore-described approach is the determination of the uniform bond stress τ_{be}. Biskinis and Fardis [11] suggest that $\tau_{be} \approx \sqrt{f_c}$. This value is adopted as the mean bond stress along L_{be}, which is about 40% to 50% of the maximum bond strength τ_{bu} of the local constitutive bond-slip law of unconfined or confined concrete, respectively, for "good" bond conditions according to Model Code 1990 [14]. The same value for τ_{be} is proposed by Lehman and Moehle [3] and Sezen and Setzler [10], who studied fixed-end rotations of RC columns subjected to cyclic loading.

By setting $\tau_{be} = \sqrt{f_c}$, the following equation for $\theta_{y,slip}$ is obtained, which is the same as the one adopted in EC8-Part3 [15].

$$\theta_{y,slip} = 0.13 \cdot \varphi_y \cdot \frac{d_{bl} \cdot f_{yl}}{\sqrt{f_c}} \tag{5}$$

Despite the convenience of the previous approach, it is not consistent with the actual local bond-slip response as it assumes constant bond stress along the anchorage length, while the slip increases quadratically from zero to the maximum value s_y at the beam-column end section. This is not consistent with the local bond-slip constitutive law presented in Fig. 2.

To overcome this limitation, a new, simple procedure is proposed herein for evaluating s_y. The method assumes that the local bond stress of an anchorage point is a general power function of the distance x from the anchorage point of zero stress, strain, and slip (Fig. 3). Hence, it is assumed:

$$\tau_b(x) = b \cdot x^c \tag{6}$$

The proposed method assumes that all points along L_{be} remain on the ascending branch of the local bond-slip law. Hence, at the end of the calculations, the following relationship should hold: $s_y < s_1$ (see Fig. 2). It is worth noting that Eq. (6) at x=0 yields $\tau_b(x)=0$, which is in accordance with the boundary condition s(x)=0 at x=0 and the local constitutive bond-slip law shown in Fig. 2.

Parameters b and c are considered unknown and will be determined in the following by satisfying local bond-slip law at $x=L_{be}$ and at an arbitrary anchorage point P at distance $x=x_P=L_{be}/m$, where m>1 (see Fig. 3). Thus, no additional assumptions are introduced for the calculation of b and c.

Application of Eq. (6) to the two points mentioned above, gives:

$$\left.\begin{array}{c} \tau_{by} = b \cdot L_{be}^{\ c} \\[2mm] \tau_{bP} = b \cdot \left(\dfrac{L_{be}}{m}\right)^c \end{array}\right\} \rightarrow \dfrac{\tau_{by}}{\tau_{bP}} = m^c \tag{7}$$

By equilibrium of an infinitesimal anchorage length dx and the boundary condition (x=0 $\rightarrow$ σ_s=0), one obtains:

$$\frac{d\sigma_s}{dx} = \frac{4}{d_{bl}} \cdot \tau_b(x) \rightarrow \sigma_s(x) = \frac{4}{d_{bl}} \cdot \frac{b}{c+1} \cdot x^{c+1} \tag{8}$$

For $x=L_{be}$, it is assumed that the steel bar is at the point of yield i.e. $\sigma_s=f_{yl}$. Solving for L_{be} and using Eq. (7), leads to:

$$f_{yl} = \frac{4}{d_{bl}} \cdot \frac{b}{c+1} \cdot L_{be}^{\ c+1} \rightarrow L_{be} = \frac{f_{yl} \cdot d_{bl} \cdot (c+1)}{4\tau_{by}} \tag{9}$$

Furthermore, since the reinforcement bar remains in the elastic region:

$$\varepsilon_s(x) = \frac{\sigma_s(x)}{E} = \frac{4}{E \cdot d_{bl}} \cdot \frac{b}{c+1} \cdot x^{c+1} \tag{10}$$

where E is the elastic modulus of steel. By ignoring the concrete strain and applying the boundary condition s(x)=0 at x=0, slip s(x) at distance x becomes:

$$s(x) = \int \varepsilon_s(x)dx = \frac{4}{E \cdot d_{bl}} \cdot \frac{b}{(c+1) \cdot (c+2)} \cdot x^{c+2} \tag{11}$$

At x=L_{be} and at x=x_P, by using Eq. (11), anchorage slips s_y and s_p respectively are related as:

$$\left. \begin{array}{l} s_y = \dfrac{4}{E \cdot d_{bl}} \cdot \dfrac{b}{(c+1) \cdot (c+2)} \cdot L_{be}^{c+2} \\[3mm] s_P = \dfrac{4}{E \cdot d_{bl}} \cdot \dfrac{b}{(c+1) \cdot (c+2)} \cdot \left(\dfrac{L_{be}}{m}\right)^{c+2} \end{array} \right\} \rightarrow \frac{s_y}{s_P} = m^{c+2} \tag{12}$$

Moreover, by considering the relationship of the bond-slip constitutive law ascending branch shown in Fig. 2 and Eq. (7), it is obtained:

$$\frac{\tau_{by}}{\tau_{bP}} = \left(\frac{s_y}{s_P}\right)^\alpha \rightarrow \left(\frac{s_y}{s_P}\right)^\alpha = m^c \tag{13}$$

Combining Eqs. (12) and (13) and since m is an arbitrary constant, it follows that:

$$\left(m^{c+2}\right)^\alpha = m^c \rightarrow \alpha \cdot (c+2) = c \rightarrow c = \frac{2\alpha}{1-\alpha} \tag{14}$$

Slip s_y can now be determined by applying Eq. (11) together with Eq. (9):

$$s_y = \frac{4}{E \cdot d_{bl}} \cdot \frac{b}{(c+1) \cdot (c+2)} \cdot L_{be}^{c+2} = \frac{f_{yl} \cdot L_{be}}{E \cdot (c+2)} = \frac{\varepsilon_y \cdot L_{be}}{(c+2)} \tag{15}$$

By further substitution of L_{be} from Eq. (9) and using the local bond-slip constitutive law, the following is obtained:

$$s_y = \frac{\varepsilon_y \cdot f_{yl} \cdot (c+1) \cdot d_{bl}}{4(c+2) \cdot \tau_{by}} = \frac{\varepsilon_y \cdot f_{yl} \cdot (c+1) \cdot d_{bl}}{4(c+2) \cdot \left(\dfrac{s_y}{s_1}\right)^a \cdot \tau_{bu}} \tag{16}$$

Finally, by substituting c from Eq. (14) and solving for s_y, it results:

$$s_y = \left(\frac{(1 + a) \cdot s_1^a \cdot \varepsilon_y \cdot f_{yl} \cdot d_{bl}}{8 \cdot \tau_{bu}} \right)^{\frac{1}{1+a}} \qquad (17)$$

It is important to note that Eq. (17) provides a closed-form solution to the calculation of s_y from the steel properties and the local bond-slip constitutive law parameters. The proposed methodology takes into account the variation of bond stress along the anchorage length and accounts for the actual shape of the local bond-slip law by introducing the constitutive parameters α, s_1 and τ_{bu}.

One of the advantages of the proposed methodology is the fact that it calculates s_y as a function of local constitutive bond-slip law parameters that have already been calibrated for different bond conditions and levels of confinement. Fig. 4(a) compares s_y predictions for different bar diameters derived by the uniform bond stress assumption $\tau_{be} = \sqrt{f_c}$ (i.e. EC8-Part 3 [15] approach) and the proposed methodology for the bond-slip constitutive law parameters corresponding to "Good" and "Other" bond conditions for the pull-out failure mode in accordance with fib Model Code 2010 [16]. Additional parameters influencing bond, like yielding, transverse stress, longitudinal cracking and cyclic loading are not examined herein. In Fig 4 concrete compressive strength is assumed equal to f_c=35MPa and steel yield strength f_{yl}=500MPa.

It can be seen that s_y predictions differ significantly for different bond conditions. The lower s_y values are predicted for concrete in "Good" bond conditions. This is expected since bond-slip ascending response is stiffer in this case. It is also interesting to compare EC8-Part 3 [15] predictions with the predictions of the proposed methodology for "Good" bond conditions (Fig. 4-right). It can be seen that the two solutions tend to converge for small bar diameters, but they deviate significantly for large diameters. This observation drives to the conclusion that no unique uniform τ_{be} can be assumed for all bar diameters, as assumed (for simplicity) in EC8-Part 3 [15].

An additional advantage of Eq. (17) is the fact that it can be readily applied to the calculation of anchorage slip for steel strains ε_{so} less than ε_y. This is achieved by simply setting in Eq. (17) ε_{so} instead of ε_y and corresponding stress $\sigma_{so} = E \cdot \varepsilon_{so}$ instead of f_{yl}.

Fig. 4(b) compares anchorage slip calculated according to EC8-Part 3 [15] and proposed approaches for the same material properties as above and bar diameter d_{bl}=8mm. It can be seen that s_y predictions from the two methodologies coincide for this bar diameter size. However, further comparison reveals that the EC8-Part 3 [15] approach may considerably underestimate anchorage slip at low steel stresses. This is because the uniform bond stress value $\tau_{be} = \sqrt{f_c}$ assumed by EC8-Part 3 [15] only applies for yielding of the longitudinal reinforcement. For lower steel stresses, lower slip values and bond stresses are expected. Hence, the EC8-Part 3 [15] approach may overestimate bond and underestimate slip of the anchorage.

Having established s_y and using the definition of the yield curvature, fixed-end rotation at yielding $\theta_{y,slip}$ can be determined as

$$\theta_{y,slip} = \varphi_y \cdot \left(\frac{(1 + a) \cdot s_1^a \cdot f_{yl} \cdot d_{bl}}{8 \cdot \varepsilon_y^a \cdot \tau_{bu}} \right)^{\frac{1}{1+a}} \qquad (18)$$

3   Fixed-end rotation at ultimate

For the calculation of fixed-end rotation at ultimate $\theta_{u,slip}$ the additional 'plastic' fixed-end rotation arising from the inelastic

part L_{bp} of the anchorage $\theta_{pu,slip}$ has to be added to $\theta_{y,slip}$. Typically, $\theta_{pu,slip}$ is significantly higher than $\theta_{y,slip}$ due to the large strains and the reduced bond capacity developed in the inelastic part of the anchorage.

To calculate accurately $\theta_{pu,slip}$ elaborate analytical methodologies are generally required like the ones mentioned in the Introduction. In addition to these methodologies, a number of researchers have made various simplifying assumptions in order to provide approximate estimates of $\theta_{pu,slip}$. The most widely adopted approach for calculating $\theta_{pu,slip}$ at onset of flexural failure is the equivalent plastic hinge length approach [17-18]. According to this approach, $\theta_{pu,slip}$ can be determined by the following equation, where $L_{sp,u}$ is the strain-penetration length at flexural failure:

$$\vartheta_{pu,slip} = \left(\varphi_u - \varphi_y \right) \cdot L_{sp,u} \tag{19}$$

Different empirical relationships, based on experimental results, have been proposed in the literature for the calculation of $L_{sp,u}$. Paulay and Priestley [17] propose the following equation (f_{yl} in MPa).

$$L_{sp,u} = 0.022 \cdot d_{bl} \cdot f_{yl} \tag{20}$$

Depending on the way the curvature of the RC member end section at flexural failure φ_u is calculated, EC8-Part 3 [15] proposes two different equations for the determination of $L_{sp,u}$ (f_{yl}, f_c in MPa), depending on the model used for confined concrete.

$$L_{sp,u} = 0.24 \cdot \frac{d_{bl} \cdot f_{yl}}{\sqrt{f_c}} \tag{21a}$$

$$L_{sp,u} = 0.11 \cdot \frac{d_{bl} \cdot f_{yl}}{\sqrt{f_c}} \tag{21b}$$

At this point, it is important to mention that the actual value of $L_{sp,u}$ cannot be treated as independent of the assumptions made for the calculation of φ_u in moment-curvature analysis. These assumptions concern the constitutive models for confined and unconfined concrete, the constitutive model for reinforcing steel, the determination of the ultimate concrete strain at failure ε_{cu} and the steel strain at failure ε_{su}. A thorough description of the assumptions made for the determination of φ_u in the three different equations of $L_{sp,u}$ (Eqs. 19 to 21) can be found in Fardis [18].

In the following, a more generic approach for determining $L_{sp,u}$ will be developed. The methodology is based on the assumption of uniform bond stress τ_{bp} inside the inelastic part of the anchorage L_{bp} (Fig. 5). The same assumption has been made by several researchers [8-13] who found good correlation of the experimental measurements and the analytical calculations. However, the previous research efforts aimed at calculating directly $\theta_{pu,slip}$ and not $L_{sp,u}$.

The aim of the proposed methodology is to propose a closed-form relationship that accounts seperately for the effects of the main parameters governing the development of the inelastic fixed-end rotations (i.e. reinforcing steel strain-hardening response, bar size, material strengths and bond-slip response between steel and surrounding concrete). In this manner, all possible combinations can be taken into consideration. Furthermore, the proposed relationship will be able to determine inelastic fixed-end rotations $\theta_{p,slip}$ at limit states prior to flexural failure. This is very important for the purposes of

performance-based design for multiple performance levels.

An important issue when calculating $\theta_{p,slip}$ is the assumption regarding the reinforcing steel strain-hardening constitutive law. Most analytical models [8-10,12] assume, for simplicity, linear hardening constitutive law. Nevertheless, a previous analytical study by Mergos and Kappos [13] has shown that the nonlinearity of the strain-hardening material law plays a significant role in the determination of $\theta_{p,slip}$. Hence, in the following, closed form relationships will be derived for both linear and nonlinear strain hardening laws of reinforcing steel.

Linear strain-hardening law

Figure 5 illustrates bond stress, steel stress and steel strain distribution along L_{bp}, where reinforcement plastic slip s_p and the corresponding fixed-end rotation $\theta_{p,slip}$ are developed. When linear strain-hardening law is assumed, steel stress after yielding σ_s is given by Eq. (22) as a function of the respective steel stress ε_s and the steel stress f_{su} and strain ε_{su} at maximum strength.

$$\sigma_s = f_{yl} + \left(f_{su} - f_{yl} \right) \cdot \frac{\left(\varepsilon_s - \varepsilon_y \right)}{\left(\varepsilon_{su} - \varepsilon_y \right)} \tag{22}$$

The anchorage length L_{bp} in the inelastic range is determined by equilibrium and by using Eq. (22). In Eq. (23), σ_{so} and ε_{so} are the steel stress and strain at the loaded end of the anchorage (Fig. 5).

$$L_{bp} = \frac{d_{bl} \cdot \left(\sigma_{so} - f_{yl} \right)}{4 \cdot \tau_{bp}} = \frac{d_{bl} \cdot \left(\varepsilon_{so} - \varepsilon_y \right)}{4 \cdot \tau_{bp}} \cdot \frac{\left(f_{su} - f_{yl} \right)}{\left(\varepsilon_{su} - \varepsilon_y \right)} \tag{23}$$

For linear strain distribution, post-yield anchorage slip s_p is easily calculated by integration as:

$$s_p = \frac{\varepsilon_{so} + \varepsilon_y}{2} \cdot L_{bp} = \frac{d_{bl} \cdot \left(\varepsilon_{so} - \varepsilon_y \right) \cdot \left(\varepsilon_{so} + \varepsilon_y \right)}{8 \cdot \tau_{bp}} \cdot \frac{\left(f_{su} - f_{yl} \right)}{\left(\varepsilon_{su} - \varepsilon_y \right)} \tag{24}$$

The respective fixed-end rotation is given by the following equation, which makes the common assumption [18] that the neutral axis depth remains approximately constant after yielding of the longitudinal reinforcement. In this equation, φ_o is the curvature at the critical end section of the RC member.

$$\vartheta_{p,slip} = \frac{s_p}{d - x_c} \approx \frac{d_{bl} \cdot \left(\varphi_o - \varphi_y \right) \cdot \left(\varepsilon_{so} + \varepsilon_y \right)}{8 \cdot \tau_{bp}} \cdot \frac{\left(f_{su} - f_{yl} \right)}{\left(\varepsilon_{su} - \varepsilon_y \right)} \tag{25}$$

The strain penetration length L_{sp} can now be calculated as:

$$L_{sp} = \frac{\vartheta_{p,slip}}{\left(\varphi_o - \varphi_y \right)} = \frac{d_{bl} \cdot \left(\varepsilon_{so} + \varepsilon_y \right)}{8 \cdot \tau_{bp}} \cdot \frac{\left(f_{su} - f_{yl} \right)}{\left(\varepsilon_{su} - \varepsilon_y \right)} \tag{26}$$

The equation above can be also written in the following form, where ε_{no} is the normalized post-yield strain ratio $\varepsilon_{no}=(\varepsilon_{so}-\varepsilon_y)/(\varepsilon_{su}-\varepsilon_y)$; in the post-yield range, ε_{no} ranges from zero to unity.

$$L_{sp} \approx \frac{\left(f_{su} - f_{yl} \right) \cdot d_{bl}}{8 \cdot \tau_{bp}} \cdot \left(\varepsilon_{no} + \frac{2\varepsilon_y}{\varepsilon_{su} - \varepsilon_y} \right) \tag{27}$$

According to Eq. (27), L_{sp} increases linearly with the normalized post-yield strain ratio ε_{no}. The same equations can be also written as:

$$L_{sp} = \frac{\left(\sigma_{so} - f_{yl} \right) \cdot d_{bl}}{8 \cdot \tau_{bp}} + \frac{\left(f_{su} - f_{yl} \right) \cdot d_{bl}}{8 \cdot \tau_{bp}} \cdot \frac{2\varepsilon_y}{\varepsilon_{su} - \varepsilon_y} \tag{28}$$

The second term of Eq. (28) can generally be neglected since $\varepsilon_y \ll \varepsilon_{su}$. In this case, L_{sp} takes the simple form of Eq. (29):

$$L_{sp} = \frac{\left(\sigma_{so} - f_{yl} \right) \cdot d_{bl}}{8 \cdot \tau_{bp}} \tag{29}$$

The post-yield fixed-end rotation $\theta_{p,slip}$ corresponding to arbitrary post-yield curvature φ_o and steel strain σ_{so} of the RC member end section can now be calculated by the standard equation:

$$\theta_{p,slip} = \left(\varphi_o - \varphi_y \right) \cdot L_{sp} = \left(\varphi_o - \varphi_y \right) \cdot \frac{\left(\sigma_{so} - f_{yl} \right) \cdot d_{bl}}{8 \cdot \tau_{bp}} \tag{30}$$

Nonlinear strain-hardening law

Nonlinearity of the strain-hardening law increases considerably the complexity of the analytical derivation of post-yield anchorage slip s_p. In the present study, the nonlinear strain-hardening law suggested by Priestley et al. [17] is examined. This is given by the following relationship:

$$\sigma_s = f_{su} - \left(f_{su} - f_{yl} \right) \cdot \left(\frac{\varepsilon_{su} - \varepsilon_s}{\varepsilon_{su} - \varepsilon_y} \right)^2 \tag{31}$$

The steel stress $\sigma_s(x)$ at a distance x from the loaded end of the anchorage is determined by equilibrium:

$$\sigma_s(x) = \sigma_{so} - \frac{4\tau_{bp}}{d_{bl}} \cdot x \tag{32}$$

Hence, the respective steel strain can be calculated by combining Eq. (31) and Eq. (32) as:

$$\varepsilon_s(x) = \varepsilon_{su} - (\varepsilon_{su} - \varepsilon_y) \cdot \sqrt{\frac{f_{su} - \sigma_{so} + 4\tau_{bp} \cdot x / d_{bl}}{f_{su} - f_{yl}}} \tag{33}$$

The anchorage slip s_p developed in L_{bp} is calculated by strain integration along this length:

$$s_p = \int_0^{L_{bp}} \left(\varepsilon_{su} - (\varepsilon_{su} - \varepsilon_y) \cdot \sqrt{\frac{f_{su} - \sigma_{so} + 4\tau_{bp} \cdot x / d_{bl}}{f_{su} - f_{yl}}} \right) dx \tag{34}$$

where L_{bp} is given by the general Eq. (35)

$$L_{bp} = \frac{d_{bl} \cdot (\sigma_{so} - f_{yl})}{4 \cdot \tau_{bp}} \tag{35}$$

Now, the equivalent plastic hinge length for anchorage slip L_{sp} can be determined by:

$$L_{sp} = \frac{\vartheta_{p,slip}}{\varphi_p} = \frac{s_p}{(\varphi_o - \varphi_y) \cdot (d - x_c)} \approx \frac{s_p}{(\varepsilon_{so} - \varepsilon_y)} \tag{36}$$

The analytical solution of Eqs. (34-36) has the following form:

$$L_{sp} = \frac{(f_{su} - f_{yl}) \cdot d_{bl}}{8 \cdot \tau_{bp}} \cdot \lambda(\varepsilon_{no}) \tag{37}$$

where:

$$\lambda(\varepsilon_{no}) = \frac{\left[1 - 3 \cdot (1 - \varepsilon_{no})^2 + 2 \cdot (1 - \varepsilon_{no})^3 \right]}{1.5 \cdot \varepsilon_{no}} \tag{38}$$

Fig. (6a) presents variation of $\lambda(\varepsilon_{no})$ with the normalized post-yield strain ratio ε_{no}. It can be seen that $\lambda(\varepsilon_{no})$ increases initially nonlinearly with ε_{no} and then tends to stabilize. In fact, when ε_{no} approaches unity, $\lambda(\varepsilon_{no})$ slightly decreases, but this can be neglected for practical applications. The maximum value of $\lambda(\varepsilon_{no})$ is approximately ¾.

More interestingly, Fig. (6b) shows the variation of λ with the normalized ratio $\sigma_{no}=(\sigma_{so}-f_{yl})/(f_{su}-f_{yl})$. In this figure, it can be seen that $\lambda(\sigma_{no})$ increases almost linearly from zero to ¾ as σ_{no} increases from zero to unity. This observation drives to the conclusion that for practical applications, Eq. (37) can be written as:

$$L_{sp} \approx \frac{3}{4} \cdot \frac{\left(\sigma_{so} - f_{yl}\right) \cdot d_{bl}}{8 \cdot \tau_{bp}} \tag{39}$$

Comparing Eqs. (29) and (39), it can be observed that they can both be written in the following general form:

$$L_{sp} = \frac{\left(\sigma_{so} - f_{yl}\right) \cdot d_{bl}}{8 \cdot \tau_{bp}} \cdot \mu \tag{40}$$

where μ is a scalar that accounts for the constitutive strain hardening law of steel (i.e. $\mu=1$ for linear hardening law and $\mu=3/4$ for quadratic hardening law). It is worth noting that for the nonlinear hardening law it is $\mu<1$. This is due to the fact that for the same σ_{no} strains along L_{bp} are generally lower than the ones corresponding to linear hardening law as evident in Fig. 5.

It is generally suggested that τ_{bp} be taken as $\tau_{bp}=\psi \cdot \sqrt{f_c}$ where ψ is a constant parameter. For example, Lehman and Moehle [3] suggest that ψ be taken equal to 0.5 for RC columns subjected to cyclic loading. Alsiwat and Saatcioglu [8] suggest that τ_{bp} be taken equal to the residual bond strength τ_{bf} of the local bond-slip constitutive law (Fig. 2). According to Model Code 2010 [16] and for pull-out failure, τ_{bf} is equal to $\sqrt{f_c}$ for "Good" and $0.5\sqrt{f_c}$ for "Other" bond conditions. However, the previous values should be modified by reduction factors accounting for reinforcement yielding, longitudinal cracking, transverse stress and cyclic loading. Hence, significantly smaller values often apply.

By substituting τ_{bp} in Eq. (40), L_{sp} takes the following general form:

$$L_{sp} = \frac{\left(\sigma_{so} - f_{yl}\right) \cdot d_{bl}}{8 \cdot \psi \cdot \sqrt{f_c}} \cdot \mu = \left[\frac{\left(\sigma_{so} / f_{yl} - 1\right)}{8 \cdot \psi} \cdot \mu\right] \cdot \frac{f_{yl} \cdot d_{bl}}{\sqrt{f_c}} \tag{41}$$

The strain penetration length at flexural failure $L_{sp,u}$ can be determined by direct substitution as:

$$L_{sp,u} = \left[\frac{\left(\sigma_{so,u} / f_{yl} - 1\right)}{8 \cdot \psi} \cdot \mu\right] \cdot \frac{f_{yl} \cdot d_{bl}}{\sqrt{f_c}} \tag{42}$$

The form of Eq. (42) can be considered as a generalization of the Eqs. (20-21) that are widely adopted for the calculation of

$L_{sp,u}$ [17-18]. The general form of all equations is the following

$$L_{sp,u} = \kappa \cdot \frac{f_{yl} \cdot d_{bl}}{\sqrt{f_c}} \qquad (43)$$

where κ is a scalar given by

$$\kappa = \frac{\left(\sigma_{so,u} / f_{yl} - 1\right)}{8 \cdot \psi} \cdot \mu \qquad (44)$$

Eqs. (43) and (44) are useful because they reveal the influence of different parameters on $L_{sp,u}$. More particularly, it is shown that $L_{sp,u}$ increases with f_{yl} and d_{bl} and decreases with $\sqrt{f_c}$. These observations are in agreement with models in existing literature. In addition, Eq. (44) shows that $L_{sp,u}$ depends on the steel stress at failure, the strain-hardening constitutive law and the general bond conditions (i.e. level of confinement, position of reinforcement, cyclic loading, longitudinal cracking, and transverse stress). The latter parameters are not taken explicitly into consideration in Eqs. (20-21).

Figure 7 illustrates the range of κ for possible values of ψ ($0.1 \leq \psi \leq 1$) and $\sigma_{so,u}/f_{yl}$ ($1.1 \leq \sigma_{so,u}/f_{yl} \leq 1.5$) for nonlinear hardening constitutive law (i.e. $\mu = 3/4$). It can be seen that κ varies from 0.01 to 0.47. It is recalled that according to EC8-Part 3 [15] κ is either 0.11 or 0.24. Hence, it is obvious that EC8-Part 3 [15] may lead to serious underestimation or overestimation of $L_{sp,u}$ and consequently $\theta_{pu,slip}$.

In Eq. (44), $\sigma_{so,u}$ is the steel stress corresponding to onset of flexural failure of the RC member end section. Usage of $\sigma_{so,u}$, instead of f_{su}, is strongly recommended for non-ductile RC members that can fail in flexure at steel stress levels significantly lower than f_{su}. This depends also on the type of the strain-hardening law. For linear hardening law, for example, it is unlikely that $\sigma_{so,u}$ will reach f_{su} even for well confined members.

In addition to the above, it should be clarified that $L_{sp,u}$ should not be used for the determination of $\theta_{p,slip}$ as it will lead to overestimation of the post-yield fixed-end rotations. Instead, the value of L_{sp} corresponding to the curvature of the member end-section should be applied. L_{sp} varies from 0 at yielding to $L_{sp,u}$ at onset of flexural failure.

4   Calibration against experimental data

In this section, the equations derived analytically for the determination of fixed-end rotations at yielding and ultimate will be calibrated against experimental data. To this goal, a set of specimens comprising 10 RC columns subjected to cyclic loading up to onset of flexural failure is utilised. For all columns, fixed-end rotations due to strain penetration in the footing were recorded during the testing procedure. Column properties and experimentally recorded fixed-end rotations are reported in Table 1; it is worth recalling herein that measurement of fixed end rotations is not easy or standardised, and hence subject to uncertainty.

Figure 8a compares the analytical predictions of $\theta_{y,slip}$ based on EC8-Part 3 Eq. (5) with the experimental measurements. It can be seen that EC8-Part 3 [15] underestimates significantly the experimental fixed-end rotations. The test-to-prediction ratio has a mean of 1.93 and median of 2.03 and coefficient of variation of 25%. Figure 8b presents the same comparison when the proposed Eq. (18) is applied. The following constitutive bond-slip parameters are adopted for this comparison: $\alpha=1.0$, $s_1=0.85$mm and $\tau_{bu}=1.25\sqrt{f_c}$. These parameters were chosen both because they provide the best correlation with the experimental results and they are consistent with the experimental measurement of the local bond-slip response under cyclic

loading conditions by Lehman and Moehle [3]. The test-to-prediction ratio has a mean of 1.00 and median of 1.03 and coefficient of variation of 23%.

Figure 9a compares the analytical predictions of $\theta_{p,slip}$ based on EC8-Part 3 (L_{sp} from Eq. (21a) and Eq. (21b)) with the experimental measurements. It can be seen that Eq. (21a) underestimates the experimental fixed-end rotations. The test-to-prediction ratio has a mean of 1.34 and median of 1.38 and coefficient of variation of 33%. On the other hand, Eq. (21b) slightly overestimates experimental measurements. More particularly, test-to-prediction ratio has a mean of 0.97 and median of 0.80 and coefficient of variation of 50%.

Figure 9b presents the same comparison when the proposed Eq. (42) is applied for L_{spu}. For the calculation of the plastic fixed-end rotation $\theta_{p,slip}$, the yield and ultimate curvature φ_y and φ_u were calculated by moment-curvature analyses and by employing the confined concrete model by Mander et al. [20] and the steel model with nonlinear hardening law suggested by Priestley et al. [17]. Critical concrete and steel strains at the ultimate limit state were assumed in accordance with the recommendations by Mander et al. [20] and Priestley et al. [17].

The following constitutive bond-slip parameters are employed for this comparison: $\psi=0.29$ and $\mu=0.75$. Parameter μ was chosen in accordance with the adopted steel model and parameter ψ was selected to provide the best fit to the experimental results. The test-to-prediction ratio has a mean of 1.10 and median of 1.00, and coefficient of variation of 54%. The predictions are slightly better than the EC8-Part 3 predictions, but still the coefficient of variation is very high. This observation reflects the level of uncertainty when calculating displacement components at the ultimate limit state. As noted earlier, the uncertainty in the experimental fixed-end rotation measurements should also have affected the quality of the comparison.

5 Conclusions

Accurate determination of fixed-end rotations at the ends of RC members due to strain penetration of the longitudinal reinforcement in the joints and/or footings, at yielding and ultimate limit states, is of primary importance for defining their inelastic structural response and is also a prerequisite for their design based on multiple performance levels.

Fixed-end rotations are either calculated by over-simplified empirical approaches that are not able to capture all aspects of strain-penetration response or by advanced numerical solutions that cannot be used in everyday engineering practice.

In an attempt to bridge this gap, this study proposed new closed-form relationships for determining strain-penetration fixed-end rotations at yielding and ultimate limit states. The relationships are based on simple, yet rational, mechanical models that increase the reliability of the results, while they also provide a better insight into the parameters affecting strain penetration.

The new relationships were first used to examine the validity of widely adopted equations in the literature and EC8-Part 3 [15] and then calibrated against experimental data from RC column specimens subjected to cyclic loading for which fixed-end rotations were recorded.

Regarding fixed-end rotation at yielding, comparison of the EC8-Part 3 equation and that proposed herein shows that the EC8-Part 3 approach is of limited validity since it assumes a uniform bond stress along the anchorage length taken always as $\tau_{be}=\sqrt{f_c}$. However, it is shown that this uniform bond stress depends on several factors like the bond conditions ("Good" and "Other" in accordance with fib Model Code 2010 [16]), level of confinement, and longitudinal bar diameter. Moreover, it is demonstrated that the EC8-Part 3 equation should not be used for steel stresses lower than the yield strength.

For the fixed-end rotation at ultimate, comparison of the EC8-Part 3 equation and that developed herein reveals again the

limitations of the EC8-Part 3 approach. It is shown that the strain-penetration length $L_{sp,u}$ used in EC8-Part 3 to calculate the plastic fixed-end rotation is not a function of only the longitudinal bar diameter, concrete strength and steel yield strength; it also depends on the steel stress at flexural failure, the constitutive strain-hardening steel law and the general bond conditions (i.e. level of confinement, position of reinforcement, cyclic loading, longitudinal cracking, and transverse stress).

Finally, comparisons with experimental results from reinforced concrete column specimens subjected to cyclic loading demonstrate that the EC8-Part 3 equations underestimate significantly the fixed-end rotation at yielding. They provide better estimations of the fixed-end rotations at ultimate, but still with high coefficients of variation. The proposed equations produce very good predictions of the fixed-end rotation at yielding. Predictions of the fixed-end rotation at the ultimate limit state are generally better than the EC8-Part 3 equations, but they are also characterised by high coefficients of variation.

6   REFERENCES

1. Ma, S.M., Bertero, V.V., Popov, E.P.: Experimental and analytical studies on hysteretic behaviour of RC rectangular and T-beam. Report EERC 76-2, University of California, Berkeley, 1976.
2. Saatcioglu, M., Ozcebe, G.: Response of reinforced concrete columns to simulated seismic loading. ACI Structural Journal, 1989, vol. 86, No. 1, pp. 3-12.
3. Lehman, D., Moehle, J.P.: Seismic performance of well confined concrete bridge columns. PEER Report 1998/01, University of California, Berkeley, 1998.
4. Viwathanatepa, S., Popov, E.P., Bertero, V.V.: Seismic behaviour of reinforced concrete interior beam-column sub-assemblages. EERC Report 79/14, University of California, Berkeley, 1979.
5. Ciampi, V., Eligehausen, R., Bertero, V.V., Popov, E.P.: Analytical model for concrete anchorages of reinforcing bars under cyclic excitations. EERC Report 82/33, University of California, Berkeley, 1982.
6. Filippou, F.: A simple model for reinforcing bar anchorages under cyclic excitations. Report EERC-85/05, University of California, Berkeley, 1985.
7. Otani, S., Sozen, M.: Behavior of multistory RC frames during earthquakes. Structural Research Series No. 392., University of Illinois, Urbana, 1972.
8. Alsiwat, J., Saatcioglu, M.: Reinforcement anchorage slip under monotonic loading. Journal of Structural Engineering, 1992, vol. 118, No. 1, pp. 2421-2438.
9. Lowes, L., Altoontash, A.: Modelling reinforced concrete beam-column joints subjected to seismic loading. Journal of Structural Engineering, 2003, vol. 129, No. 12, pp. 1686-1697.
10. Sezen, H., Setzler, E.J.: Reinforcement slip in reinforced concrete columns anchorage slip under monotonic loading. ACI Structural Journal, 2008, vol. 105, No. 3, pp. 280-289.
11. Biskinis, D., Fardis, M.N.: Deformations at flexural yielding of members with continuous or lap-spliced bars. Structural Concrete, 2010, vol. 11, No.3, pp. 127-138.
12. Biskinis, D., Fardis, M.N.: Flexure-controlled ultimate deformations of members with continuous or lap-spliced bars. Structural Concrete, 2010, vol. 11, No.2, pp. 93-108.
13. Mergos, P.E., Kappos, A.J.: A gradual spread inelasticity model for RC beam-columns accounting for flexure, shear and anchorage slip. Engineering Structures, 2012, vol. 44, pp. 94-106.
14. CEB: CEB-FIP Model Code 1990. Design Code. Thomas Telford, London, 1993, p.437.
15. European Committee for Standardization: Eurocode 8: Design provisions of structures for earthquake resistance - Part 3: Assessment and retrofitting of buildings. Brussels, 2005.
16. fib: Model Code 2010. Final Draft, volume 1, fib Bull. 56 .
17. Paulay, T., Priestley, M.J.N.: Seismic design of reinforced concrete and masonry buildings. New York: J. Wiley and Sons, 1992.
18. Fardis, M.N.: Seismic design, assessment and retrofitting of concrete buildings. Dordrect: Springer 2009.
19. Calderone, A.J., Lehman, D.E., Moehle, J.P.: Behaviour of reinforced concrete bridge columns having varying aspect ratios and varying lengths of confinements. PEER Report 2000/08, University of California, Berkeley, 2000.
20. Mander, J.B., Priestley M.J.N., Park, R.: Theoretical stress-strain model for confined concrete. Journal of Structural Engineering, 1986, vol. 114, No. 8, pp. 1804-1825.

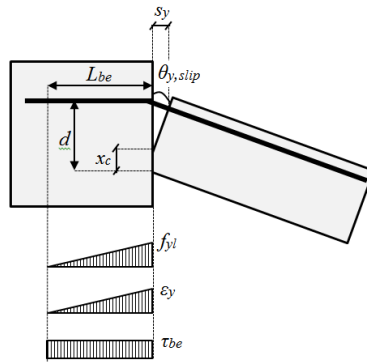**Fig. 1.** Determination of fixed-end rotation at yielding by assuming uniform bond stress distribution
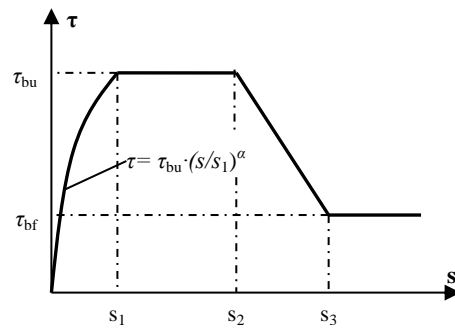
Fig. 2. Local constitutive bond-slip law (adopted by Model Code 2010 [16])
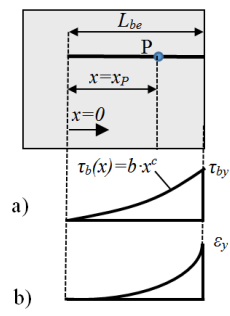
Fig. 3. Proposed solution methodology for fixed-end rotation at yielding: a) bond stress distribution and b) steel strain distribution along L_{be}
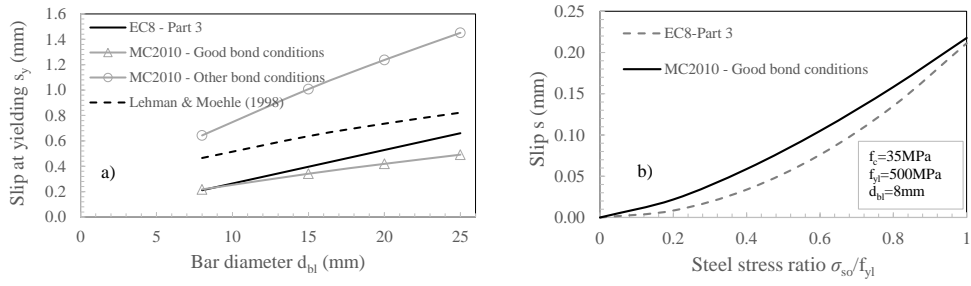
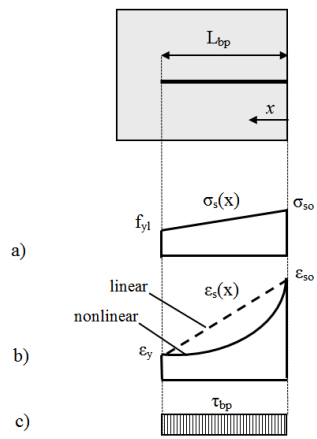**Fig. 4.** Comparison of proposed model (with τ-s from MC2010) and relationships from the literature: (a) s_y vs. d_{bl}; (b) s vs. σ_{so}/f_{yl}

Fig. 5. Proposed solution methodology for inelastic fixed-end rotations: a) steel stress distribution; b) steel strain distribution and c) bond distribution along L_{bp}
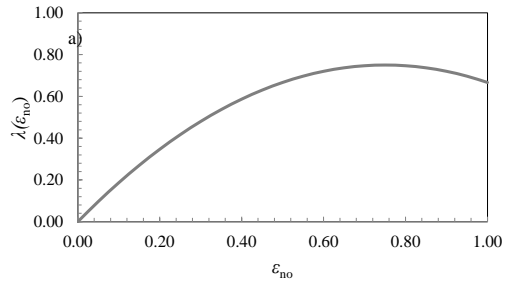
Fig. 6: Variation of λ with a) ε_{no}; b) σ_{no}
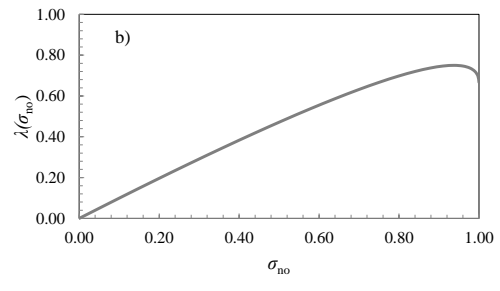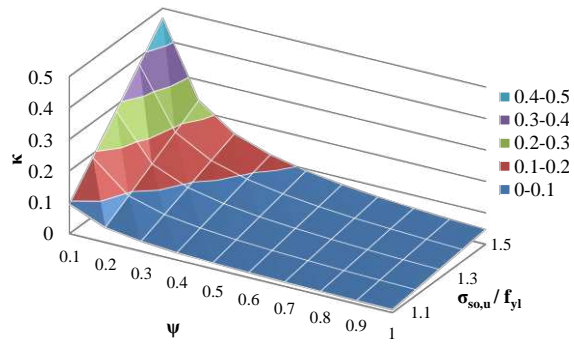
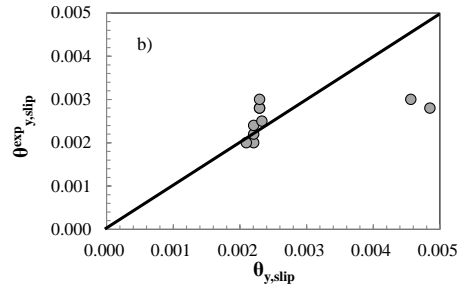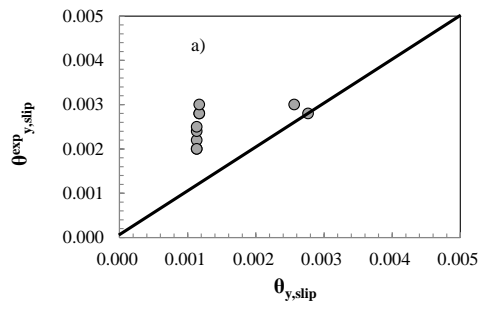**Fig. 7**: Range of values of κ for typical values of ψ and $\sigma_{so,u}/f_{yl}$

Fig. 8: Comparison of $\theta_{y,slip}$ experimental data with analytical predictions by a) EC8-Part 3 [15]; b) proposed methodology
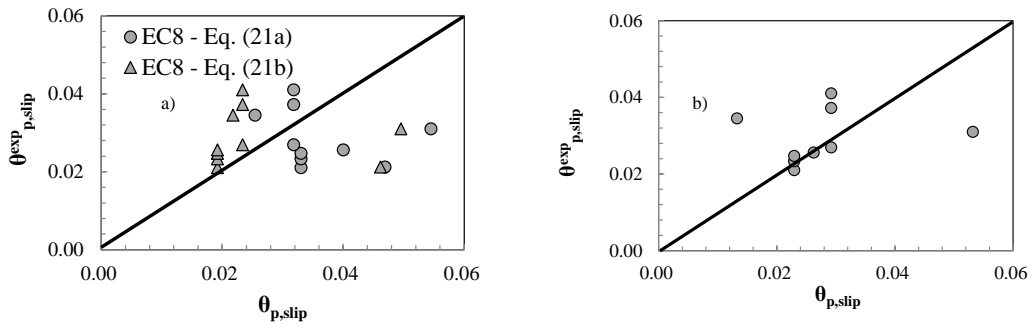
Fig. 9: Comparison of $\theta_{p,slip}$ experimental data with analytical predictions by a) EC8-Part 3 [15]; b) proposed methodology

Table 1 Experimentally recorded fixed-end rotations of RC column specimens

Reference	Specimen	Cross section	h (mm)	f_c (MPa)	f_{yl} (MPa)	d_{bl} (mm)	L_s (mm)	$\theta^{exp}_{y,slip}$ (rad)	$\theta^{exp}_{u,slip}$ (rad)	$\theta^{exp}_{p,slip}$ (rad)
[3]	415	Circular	610	31	462	15.9	2440	0.002	0.023	0.021
[3]	815	Circular	610	31	462	15.9	4880	0.0022	0.0255	0.0233
[3]	1015	Circular	610	31	462	15.9	6100	0.0024	0.0271	0.0247
[3]	407	Circular	610	31	462	15.9	2440	0.002	0.0276	0.0256
[3]	430	Circular	610	31	462	15.9	2440	0.0025	0.037	0.0345
[19]	328	Circular	610	34.5	441	19.05	1828.8	0.0028	0.04	0.0372
[19]	828	Circular	610	34.5	441	19.05	4876.8	0.0028	0.0297	0.0269
[19]	1028	Circular	610	34.5	441	19.05	6096	0.003	0.044	0.041
[2]	U4	Square	350	32	438	25	1000	0.0028	0.024	0.0212
[2]	U6	Square	350	37.3	438	25	1000	0.003	0.034	0.031